

Thermal transport in hollow metallic microlattices

Cite as: APL Mater. 7, 101108 (2019); <https://doi.org/10.1063/1.5114955>

Submitted: 13 June 2019 . Accepted: 13 September 2019 . Published Online: 09 October 2019

Shiva Farzinazar , Tobias Schaedler, Lorenzo Valdevit, and Jaeho Lee 



View Online



Export Citation



CrossMark

ARTICLES YOU MAY BE INTERESTED IN

[Investigation of thermal conduction in symmetric and asymmetric nanoporous structures](#)
Journal of Applied Physics **122**, 244305 (2017); <https://doi.org/10.1063/1.5006818>

[In praise and in search of highly-polarizable semiconductors: Technological promise and discovery strategies](#)
APL Materials **7**, 100902 (2019); <https://doi.org/10.1063/1.5124795>

[Regulation of electron-hole recombination kinetics on uniform metal-semiconductor nanostructures for photocatalytic hydrogen evolution](#)
APL Materials **7**, 100702 (2019); <https://doi.org/10.1063/1.5099666>

additive manufacturing epitaxial crystal growth cerium oxide polishing powder silver nanoparticles sputtering targets



THE ADVANCED MATERIALS MANUFACTURER®

deposition slugs OLED Lighting spintronics solar energy

GDC li-ion battery electrolytes 99.999% ruthenium spheres

endoheedral fullerenes copper nanoparticles diamond micropowder

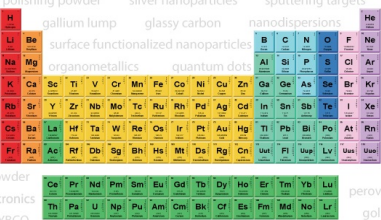
CIGS MBE grade materials palladium catalysts flexible electronics

beta-barium borate borosilicate glass dysprosium pellets YBCO

pyrolytic graphite 3d graphene foam indium tin oxide mesoporous silica

raman substrates sapphire windows tungsten carbide InGaAs

barium fluoride carbon nanotubes lithium niobate scandium powder



gallium lump glassy carbon nanodispersions

surface functionalized nanoparticles organometallics quantum dot

III-IV semiconductors CVD precursors europium phosphors

InAs wafers laser crystals ultra high purity materials MOFs

rare earth metals photovoltaics refractory metals MOCVD

superconductors transparent ceramics ultra high purity silicon

*American Elements opens up a world of possibilities so you can **Now Invent!***

Over 15,000 certified high purity laboratory chemicals, metals, & advanced materials and a state-of-the-art Research Center. Printable GHS-compliant Safety Data Sheets. Thousands of new products. And much more. All on a secure multi-language "Mobile Responsive" platform.

perovskite crystals yttrium iron garnet alternative energy h-BN

gold nanocubes graphene oxide macromolecules photonics

rhodium sponge fiber optics beamsplitters infrared dyes zeolites

fused quartz metallocenes platinum ink buckyballs Ti-6Al-4V

Now Invent.™
The Next Generation of Material Science Catalogs

www.americanelements.com



Thermal transport in hollow metallic microlattices

Cite as: APL Mater. 7, 101108 (2019); doi: 10.1063/1.5114955

Submitted: 13 June 2019 • Accepted: 13 September 2019 •

Published Online: 9 October 2019



Shiva Farzinazar,¹ Tobias Schaedler,² Lorenzo Valdevit,^{1,3} and Jaeho Lee^{1,a)}

AFFILIATIONS

¹Department of Mechanical and Aerospace Engineering, University of California, Irvine, California 92697, USA

²HRL Laboratories Limited Liability Company, Malibu, California 90265, USA

³Department of Materials Science and Engineering, University of California, Irvine, California 92697, USA

^{a)}Author to whom correspondence should be addressed: jaeholee@uci.edu

ABSTRACT

While over the past decade architected cellular materials have been shown to possess unique mechanical properties, their thermal properties have received relatively little attention. Here, we investigate thermal transport in hollow nickel microlattices as a function of temperature and mechanical loading using infrared thermography. The effective thermal conductivity of hollow nickel microlattices with 99.9% porosity and 1 μm layer thickness is as low as $0.049 \text{ W m}^{-1} \text{ K}^{-1}$ at 320 K and increases to $0.075 \text{ W m}^{-1} \text{ K}^{-1}$ at 480 K, an increase we attribute to internal thermal radiation. By measuring the emissivity and using the Stephan-Boltzmann law, we estimate the contribution of thermal radiation in the effective thermal conductivity to range from 20% at 320 K to 49% at 480 K. The high porosity of microlattices strongly limits solid conduction and makes surface radiation very important in thermal transport. We further explore the impact of the strut surface condition by comparing hollow doped nickel microlattices with a smooth surface to those with a rough surface: the emissivity increases from 0.24 to 0.43, leading to increased thermal radiation contributions of 41% at 320 K to 58% at 480 K. Under mechanical loading, as the strain increases from 0% to 50%, decreasing the angle between the struts and the horizontal plane from 60° to 38° , the effective thermal conductivity decreases from $0.049 \text{ W m}^{-1} \text{ K}^{-1}$ to $0.016 \text{ W m}^{-1} \text{ K}^{-1}$. These findings indicate that architected cellular materials provide an excellent platform to control thermal properties independently on mechanical properties and to potentially develop thermal and thermomechanical metamaterials.

© 2019 Author(s). All article content, except where otherwise noted, is licensed under a Creative Commons Attribution (CC BY) license (<http://creativecommons.org/licenses/by/4.0/>). <https://doi.org/10.1063/1.5114955>

I. INTRODUCTION

Recent advances in additive manufacturing have led to architected materials with strongly hierarchical topologies and fascinating properties such as ultrahigh strength, ultrahigh surface-to-volume ratio, and ultralow density.^{1–4} High precision additive manufacturing techniques such as self-propagating photopolymer waveguides (SPPW),⁵ direct laser writing (DLW),^{6,7} and projection microsteolithography (P μ SL)⁸ have enabled the fabrication of lattices with submicron feature sizes^{9–12} and high porosity up to 99.9%. These microlattices and nanolattices can offer extremely high specific stiffness and strength,¹³ or full recovery from very large compressive strains (>50%) and associated structural damping,^{2,3} despite their constituent materials being inherently brittle. When designed and fabricated at low relative densities, these architected materials are anticipated to provide an exceptionally low thermal conductivity, even with highly conductive constituents.¹⁴ This combination of mechanical and thermal properties could make these materials ideal

for thermal insulation in a number of aerospace systems, from gas turbines to hypersonics, where a combination of high strength and low thermal conductivity is desirable. Schaedler *et al.*² demonstrated that hollow nickel microlattices can be fabricated with a combination of SPPW and electroless plating to span more than 7 orders of magnitude in length scale, which provides excellent control over the design and resultant properties.¹⁵ Furthermore, high recoverability upon each cyclic loading² creates an opportunity for thermal control via modulation of the applied force. The thermal properties of these microlattices are explored in this work. While the unique mechanical properties of architected microlattices have been actively investigated in recent literature,^{1–3,5,13,15–17} the associated thermal properties, including the capability of manipulating heat flows, have received little attention. Dou *et al.* measured the thermal conductivity of nanoscale lattices¹⁸ using electrical resistance thermometry while heating the structure from 95 to 300 K with a microfabricated heater in contact with the lattice. However, neither Dou *et al.* nor other studies on the thermal characterization of highly porous

media^{19–22} have explored the effect of mechanical loading on thermal transport, the variation of thermal conductivity at high temperatures, or the contribution of radiation to the effective thermal conductivity. We developed a novel methodology, using a noncontact temperature measurement approach, to minimize the errors created by other in-contact metrologies for thermal conductivity measurement of highly porous structures. This approach allows us to decouple the dominant heat transfer modes in highly porous structures—conduction and radiation—and to study their contributions individually. Additionally, using this methodology eliminates the role of the thermal contact resistance between the hollow nickel microlattice and its adjacent objects. Here, we report the effective thermal conductivity of hollow nickel microlattices as a function of temperature and mechanical loading.

II. MATERIALS AND METHODS

All samples studied here are fabricated by HRL Laboratories with the SPPW method. This technology enables the formation of the three-dimensional hollow nickel microlattices from a two-dimensional exposure mask.⁵ The fabrication procedure consists of fabricating the polymeric sacrificial layer, coating the sample with electroless doped Ni deposition (93% Ni and 7% P by weight), and etching the sacrificial core, ultimately resulting in a series of octahedral unit cells with hollow struts that are connected at nodes^{15,23,24} [Fig. 1(a)]. The coating material was not annealed after the deposition, resulting in a supersaturated solid solution of phosphorous in a crystalline nickel lattice. This technique results in feature sizes in the order of 1 μm . Considering the mean free path of nickel in the range of 6 nm,²⁵ the contribution of boundary scattering is minimal, and therefore, macroscopic heat transfer governs the energy balance equations. All lattice feature dimensions have been characterized using the Scanning Electron Microscopy (SEM), and the results are summarized in Table 1 (supplementary material, Sec. 1).

The thermal conductivity measurement was performed using the setup demonstrated in Fig. 1(c). The sample was assembled between two quartz disks, and the stack was placed between a heat source and an anchored heat sink in a vacuum environment. A

JANIS VPF-800 vacuum chamber was utilized for housing the sample, and an Edwards T-station 75 turbopump was used for maintaining the vacuum level below 10^{-5} Torr (high vacuum range) for each measurement. By turning on the heater, the heat propagates from the top toward the anchored heat sink. The hollow nickel microlattice is an effective medium, and the nonlinear temperature gradient is a result of both conduction and radiation heat losses, as confirmed by finite element simulations [Fig. 1(d)]. The incoming heat flux was calculated using the known thermal properties of the quartz disk and the temperature gradient within the quartz. Details on the emissivity calibration for temperature measurements are provided in Sec. 2 of the supplementary material. The effective thermal conductivity of the lattice was calculated using the temperature gradient in IR images [Fig. 1(b)] and the incoming heat flux (supplementary material, Sec. 3).

Various theoretical and empirical correlations were used in the literature for modeling the thermal conductivity of 2-dimensional composites.^{26–28} Ashby²⁹ proposed that the conduction contribution in a connected network of struts should incorporate the thermal properties of the constituent material, the topology of the unit cell, and volume fraction of the structure. Therefore, the effective thermal conductivity of cellular solids inside the vacuum environment can be described as

$$k_c = \frac{1}{3} \cdot \nu \cdot k_{sol}, \quad (1)$$

where ν is the volume fraction of the solid (also known as the relative density of the architected material), and k_{sol} is the intrinsic thermal conductivity of the constituent solid. The factor 1/3 represents the fraction of struts aligned with the heat flux direction. As for the microlattices under consideration this fraction equals $\sin \theta$, we express the conductive contribution to the effective thermal conductivity as

$$k_{cond} = \sin \theta \cdot \nu \cdot k_{sol}, \quad (2)$$

where the volume fraction of solid, ν , can be expressed at first order as³⁰

$$\nu = 2\pi \cdot D \cdot t / (\cos^2 \theta \cdot \sin \theta \cdot l^2), \quad (3)$$

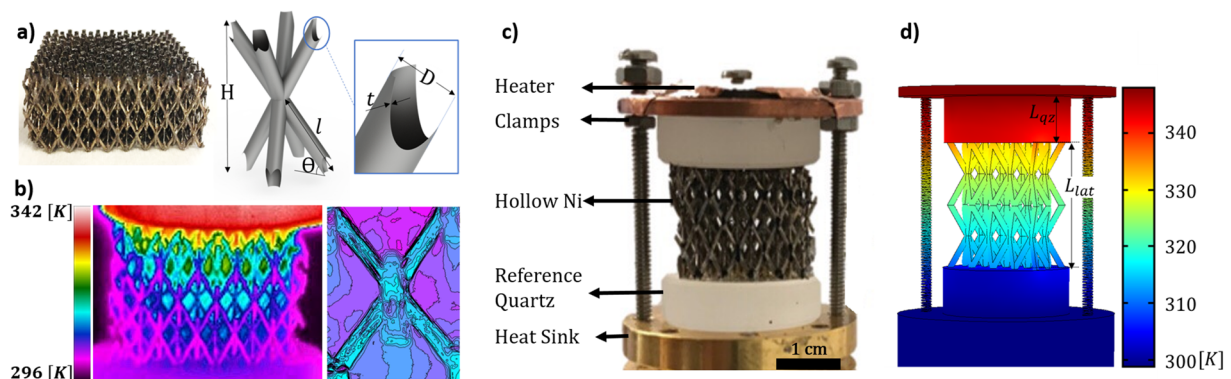


FIG. 1. (a) The hollow doped nickel microlattice in addition to the unit cell with geometric features. θ was set to 60° while ranges of 9–10.5 mm for H , 1–2 μm for thickness, and 500–650 μm for the diameter were explored. (b) Corresponding IR image of the experimental setup along with the temperature distribution of a unit cell. (c) The experimental setup used for thermal conductivity measurement of hollow nickel microlattices. The applied clamps are used for changing the height of the heater in the case of thermal conductivity measurement under compression. (d) The FEM simulation of the whole setup illustrating the one directional heat transfer throughout the stack.

where D , t , and l are the diameter, thickness, and length of the hollow struts, respectively, and θ is the angle of the struts with the horizontal plane, as illustrated in Fig. 1(a).

The effective thermal conductivity is a summation of the conduction and radiation contributions, k_{cond} and k_{rad} . Following the approach suggested by Zhao *et al.*,³¹ the radiative thermal conductivity is calculated based on the radiation heat flux which is a function of the view factors, radiosity, calibrated emissivity, volume fraction, and temperature. The effective thermal conductivity is then a summation of the conduction and radiation contributions. By utilizing the diffraction theory and the geometric optic laws, we used the Rosseland mean coefficient³² for the radiative analytical model. The effect of strut shapes and their angular configuration on irradiance was employed using the view factors. Details on the derivation of view factors are provided in Sec. 5 of the [supplementary material](#). The radiation contribution to the conductivity was calculated based on the surface to volume ratio of hollow nickel microlattices. The calculation procedure for emission and reflection heat fluxes in the vertical direction [$(q_{rad,Y})_{emission}$ and $(q_{rad,Y})_{reflection}$] can be found in the [supplementary material](#), Sec. 4.

Hence, the effective thermal conductivity can be expressed as

$$k_{eff} = k_{cond} + k_{rad} = \sin \theta \cdot v \cdot k_{sol} + [(q_{rad,Y})_{emission} + (q_{rad,Y})_{reflection}] / (\Delta T \cdot L_{lat}) \quad (4)$$

with ΔT as the vertical temperature gradient in the sample and L_{lat} depicted in Fig. 1(d).

III. RESULTS AND DISCUSSION

A. Compression dependent thermal conductivity

High recoverability after compressive deformation of hollow nickel microlattices² motivated us to measure the effective thermal conductivity under varying levels of compression. Each compression cycle creates a discontinuity inside the medium as a result of crack initiation, especially at nodes which are more prone to crack formation. We discovered that after three loading-unloading cycles, the crack initiation saturates ([supplementary material](#), Sec. 5); thus, we were able to study the impact of strain as an individual factor. Herein, the strain is defined as the ratio of the height reduction in the sample to the initial height (engineering strain). The measurement was performed in a vacuum environment, and the effective thermal conductivity was measured under compression from 0% up to 50% strain for the samples with a volume fraction of 0.09%.

By increasing the force, unit cells start sliding on top of the glass in the lateral space domain and obtain a smaller θ each time. The change in θ is not uniform across the structure; as a result, we report each strain cycle with a representative average θ value [Fig. 2(a)] ranging from $60^\circ \pm 2^\circ$ for the 0% strain and $38^\circ \pm 6^\circ$ for the 50% strain. As illustrated in Fig. 2(b), increasing the strain causes a reduction in the effective thermal conductivity. This effect can be rationalized by noting that the applied strain reduces the strut angle θ , thus affecting the conductive contribution to the effective conductivity both directly [Eq. (2)] and

through the volume fraction [Eq. (3)]. While the volume fraction is a concave function of θ , the effective thermal conductivity keeps decreasing by decreasing the θ value, ultimately resulting in the trend displayed in Fig. 2(b). The dashed lines represent our analytical solution, obtained using Eq. (4). Additionally, reducing θ leads to the reduction of view factors in radiation contribution. The reduction is caused due to the decrease in angle, leading to reduced radiative interaction between struts and surrounding. The radiation contribution as a function of θ illustrates how the increase in view factors cause a significant input of radiative conductivity on the overall effective thermal conductivity at 320 K, Fig. 2(c).

B. Temperature-dependent thermal conductivity

Even though the intrinsic thermal conductivity of metals does not change significantly at temperatures higher than ambient,³³ the radiative thermal conductivity and the resultant effective thermal conductivity strongly depend on the temperature, Fig. 3(a). The dashed lines in Fig. 3 demonstrate the radiative conductivity modeling of the hollow nickel microlattices, and their slope is derived by the surface emissivity and surface to volume ratio of the samples. Hollow nickel microlattices with the volume fraction of 0.09% exhibit a significant radiation contribution of $20.40\% \pm 4.46\%$ and 40.50 ± 2.23 in the case of the polished and rough samples, respectively [Fig. 3(b)]. This phenomenon is mainly due to the high surface to volume ratio ($\sim 1000 \text{ mm}^{-1}$) of these samples, which signifies the radiation contribution even at low temperatures. The sample with the 0.15% volume fraction shows a higher thermal conductivity compared to the polished sample with a similar surface emissivity ($\epsilon_{polished, v=0.15\%} = 0.21 \pm 0.02$). This is mainly due to the increase in the conduction contribution as a result of increasing the solid constituent of the material. The sample with the rough surface finish demonstrates the highest effective thermal conductivity value at 560 K among all samples due to the highest thermal conductivity growth rate governed by larger surface emissivity. These findings indicate that surface finish could be another approach to change the effective thermal properties at ultra-low-density ranges without affecting the mechanical properties for high temperature applications.

C. Thermomechanical evaluation of hollow nickel microlattices

Using the reported mechanical properties of hollow nickel microlattices,^{2,30} we examined the thermomechanical performance of these structures on a plot of specific Young's modulus vs effective thermal conductivity, Fig. 4(b). A shift in the order of $1000 \text{ W m}^{-1} \text{ K}^{-1}$ in thermal conductivity is made from the metal section all the way to the foams as a result of exploiting the architecture of the nickel in a lattice structure. The scaling law of the Young's modulus for these structures follows as $E \sim v^2$ in contrast to its competitors in the ultralight aerogel and carbon nanotube (CNT) foam family ($E \sim v^3$); therefore, the architectural order of these microlattices² makes their relative compressive modulus privileged compared to silica aerogels,³⁴ open cell polymer foams,³⁵ and CNT foams³⁶ in the similar volume fraction range. Direct correlation between the effective Young's modulus and effective thermal

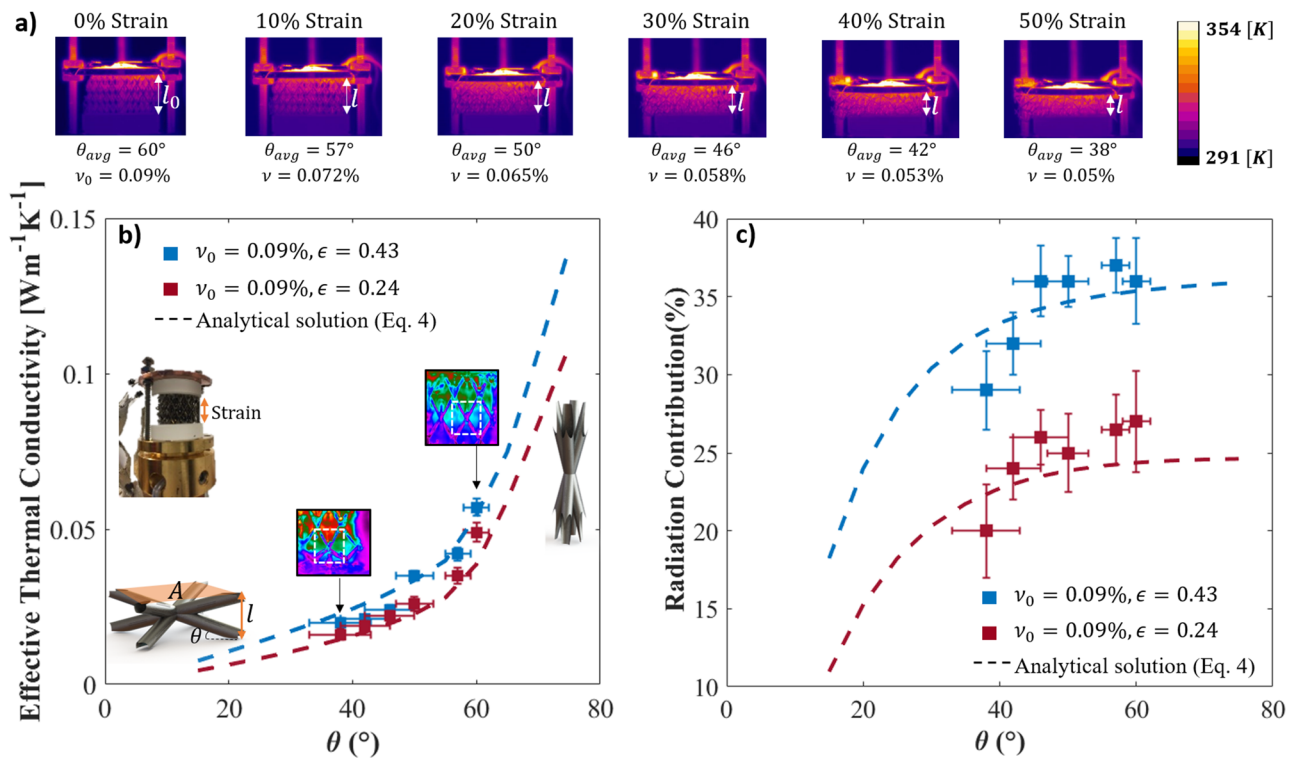


FIG. 2. (a) The strain is defined as $\delta = (l_0 - l)/l_0$ in which l is identified in each image. Increasing the applied force causes the unit cells to slide, reducing θ in a nonuniform manner. The representative average θ value and volume fraction for each compression cycle are reported. (b) The experimental data along with analytical modeling for 2 samples with the same volume fraction and different surface finishes are illustrated as a function of θ on the left axis. The analytical model is verified by the FEM results for unit cells with angles ranging from 15° to 75° . Increasing strain results in a decrease in the structural length along with an increase in the structure's area. Consequently, the Fourier equation explains the decrease in the conduction contribution of the effective thermal conductivity ($k_{eff} = ql/\Delta TA$). (c) The radiation contribution is defined as the ratio of the radiative thermal conductivity over the effective conductivity. Reducing θ leads to a lower contribution of radiation, correlated with the reduction of the effective thermal conductivity.

conductivity with the volume fraction results in designated areas in Fig. 4(b). These ellipses are evaluated to be a function of the volume fraction and bulk properties of the constituent material (E_{sol} , ρ_{sol} , k_{sol} in which E_{sol} and ρ_{sol} are the Young's modulus and the

density of the bulk material, respectively). Figure 4(b) illustrates a design space for reaching an ultralow thermal conductivity value by modifying the volume fraction and surface finish of the lattice structure.

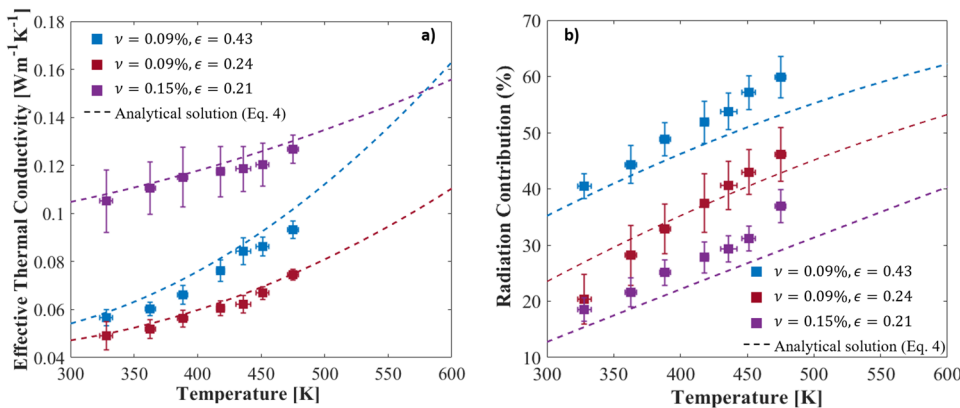


FIG. 3. (a) The effective thermal conductivity of the samples with 0.09% and 0.15% volume fraction values was measured as a function of temperature. The difference between the blue and red data points illustrates the contribution of surface emissivity in samples sharing the same volume fraction. The slope of the dashed lines shows the rate of growth in the effective thermal conductivity as a result of radiation contribution. (b) The radiation contribution of all samples is derived as a function of temperature, while the dashed lines demonstrate the analytical modeling.

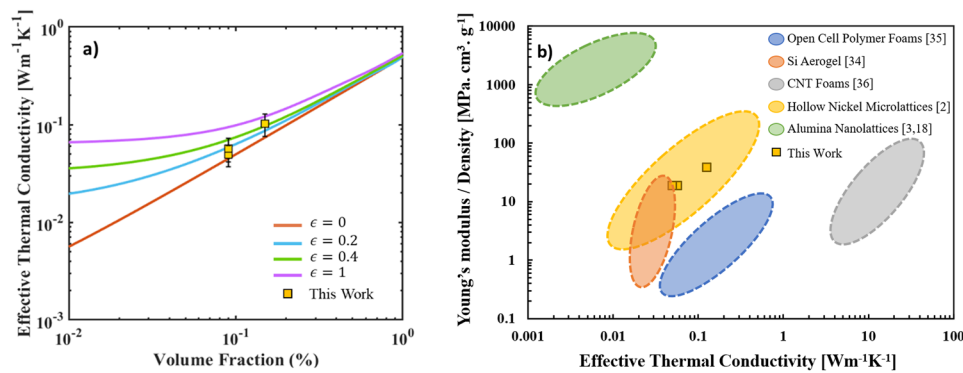


FIG. 4. (a) The design space demonstrates the potential effective thermal conductivity values as a function of volume fraction and surface emissivity using Eq. (4). Beyond 1% volume fraction, all lines (representing different emissivity values) converge, demonstrating conduction as the main mode of heat transfer. Comparatively, below 1% volume fraction, radiation contribution signifies, exposing the difference in the effective thermal conductivity at a specific volume fraction. (b) Hollow nickel microlattice placement in the material property plot of specific Young's modulus vs effective thermal conductivity. Dashed outlines indicate the allocated region for each material using the Ashby model for cellular solids,²⁹ while markers represent the measured data points. Hollow nickel microlattices can obtain higher mechanical strength and lower effective thermal conductivity compared to other mesoscale cellular materials.

IV. CONCLUSIONS

Hollow nickel microlattices offer not only volume fractions up to an order of magnitude lower than conventional materials but also offer a specific Young's modulus that is superior to that of conventional ultralight materials. Beyond the well known mechanical advantages, we have shown the thermal properties of the microlattices by measuring the effective thermal conductivity as a function of compression and temperature. The hollow nickel microlattices possess a high surface area to volume ratio; this yields a significant radiation contribution that is apparent even at temperatures where radiation is not typically considered as a dominant mode of heat transfer. Our measurements demonstrated that the increasing contribution of radiation subsequently increases the effective thermal conductivity of the lattice structure as the temperature is raised. Analytical modeling highlighted the competing effects of conduction and radiation in the structure, demonstrating that even an emissivity value of 0.43 leads to radiation becoming the dominant mode at a temperature as low as 420 K. Furthermore, measuring the effective thermal conductivity under compressive strain values ranging from 0% to 50% resulted in a 67% drop in the effective thermal conductivity; this is due to the change of angle in the struts and reduction of the volume fraction of structure. These findings indicate that architected cellular materials provide an excellent platform to control thermal properties as well as mechanical properties and to potentially develop thermal metamaterials.

SUPPLEMENTARY MATERIAL

Detailed description on methodology, modeling, and specifications of the samples can be found in the [supplementary material](#).

ACKNOWLEDGMENTS

The authors would like to thank HRL Laboratories for sample fabrication and helpful discussions. S.F. wants to acknowledge

Jonathan Sullivan, Laia Ferrer Argemi, and Mohammad H. Asadian for their help on building the setup and proof-reading. This material is based upon work supported by the National Aeronautics and Space Administration under ESI Grant No. 80NSSC18K0259 issued through the Mission Directorate.

REFERENCES

- J. Bauer, S. Hengsbach, I. Tesari, R. Schwaiger, and O. Kraft, "High-strength cellular ceramic composites with 3D microarchitecture," *Proc. Natl. Acad. Sci. U. S. A.* **111**(7), 2453–2458 (2014).
- T. A. Schaedler, A. J. Jacobsen, A. Torrents *et al.*, "Ultralight metallic microlattices," *Science* **334**(6058), 962–965 (2011).
- L. R. Meza, S. Das, and J. R. Greer, "Strong, lightweight, and recoverable three-dimensional ceramic nanolattices," *Science* **345**(6202), 1322–1326 (2014).
- X. Zheng, H. Lee, T. H. Weisgraber *et al.*, "Ultralight, ultrastiff mechanical metamaterials," *Science* **344**(6190), 1373–1377 (2014).
- A. J. Jacobsen, W. Barvosa-Carter, and S. Nutt, "Micro-scale truss structures formed from self-propagating photopolymer waveguides," *Adv. Mater.* **19**(22), 3892–3896 (2007).
- S. Maruo, O. Nakamura, and S. Kawata, "Three-dimensional microfabrication with two-photon-absorbed photopolymerization," *Opt. Lett.* **22**(2), 132 (1997).
- A. Selimis, V. Mironov, and M. Farsari, "Direct laser writing: Principles and materials for scaffold 3D printing," *Microelectron. Eng.* **132**, 83–89 (2014).
- X. Zheng, J. Deotte, M. P. Alonso *et al.*, "Design and optimization of a light-emitting diode projection micro-stereolithography three-dimensional manufacturing system," *Rev. Sci. Instrum.* **83**(12), 125001 (2012).
- J. Bauer, L. R. Meza, T. A. Schaedler, R. Schwaiger, X. Zheng, and L. Valdevit, "Nanolattices: An emerging class of mechanical metamaterials," *Adv. Mater.* **29**(40), 1701850 (2017).
- X. Zheng, W. Smith, J. Jackson *et al.*, "Multiscale metallic metamaterials," *Nat. Mater.* **15**, 1100 (2016).
- L. C. Montemayor and J. R. Greer, "Mechanical response of hollow metallic nanolattices: Combining structural and material size effects," *J. Appl. Mech.* **82**, 071012 (2015).
- T. Bückmann, N. Stenger, M. Kadic *et al.*, "Tailored 3D mechanical metamaterials made by dip-in direct-laser-writing optical lithography," *Adv. Mater.* **24**, 2710–2714 (2012).
- J. Bauer, A. Schroer, R. Schwaiger, and O. Kraft, "Approaching theoretical strength in glassy carbon nanolattices," *Nat. Mater.* **15**(4), 438–443 (2016).

- ¹⁴E. Sadeghi, S. Hsieh, and M. Bahrami, "Thermal conductivity and contact resistance of metal foams," *J Phys. D: Appl. Phys.* **44**(12), 125406 (2011).
- ¹⁵A. Torrents, T. A. Schaedler, A. J. Jacobsen, W. B. Carter, and L. Valdevit, "Characterization of nickel-based microlattice materials with structural hierarchy from the nanometer to the millimeter scale," *Acta Mater.* **60**(8), 3511–3523 (2012).
- ¹⁶Z. C. Eckel, C. Zhou, J. H. Martin, A. J. Jacobsen, W. B. Carter, and T. A. Schaedler, "Additive manufacturing of polymer-derived ceramics," *Science* **351**(6268), 58–62 (2016).
- ¹⁷J. J. do Rosário, E. T. Lilleodden, M. Waleczek *et al.*, "Self-assembled ultra high strength, ultra stiff mechanical metamaterials based on inverse opals," *Adv. Eng. Mater.* **17**, 1420–1424 (2015).
- ¹⁸N. G. Dou, R. A. Jagt, C. M. Portela, J. R. Greer, and A. J. Minnich, "Ultralow thermal conductivity and mechanical resilience of architected nanolattices," *Nano Lett.* **18**, 4755 (2018).
- ¹⁹N. Babcsán, I. Mészáros, and N. Hegman, "Thermal and electrical conductivity measurements on aluminum foams," *Materialwiss. Werkstofftech.* **34**, 391–394 (2003).
- ²⁰E. N. Schmierer, "Metal foam model for thermal applications," *J. Heat Transfer* **128**, 1194 (2006).
- ²¹V. V. Calmidi and R. L. Mahajan, "The effective thermal conductivity of high porosity fibrous metal foams," *J. Heat Transfer* **121**, 466–471 (1999).
- ²²X. Xiao, P. Zhang, and M. Li, "Effective thermal conductivity of open-cell metal foams impregnated with pure paraffin for latent heat storage," *Int. J. Therm. Sci.* **81**(1), 94–105 (2014).
- ²³L. Valdevit, S. W. Godfrey, T. A. Schaedler, A. J. Jacobsen, and W. B. Carter, "Compressive strength of hollow microlattices: Experimental characterization, modeling, and optimal design," *J. Mater. Res.* **28**(17), 2461–2473 (2013).
- ²⁴S. Godfrey and L. Valdevit, "A novel modeling platform for characterization and optimal design of micro-architected materials," in *53rd AIAA/ASME/ASCE/AHS/ASC Structures, Structural Dynamics and Materials Conference, April 2012* (AIAA/ASME/ASCE/AHS/ASC, 2012).
- ²⁵D. Gall, "Electron mean free path in elemental metals," *J. Appl. Phys.* **119**, 085101-1–085101-5 (2016).
- ²⁶R. C. Progelhof, J. L. Throne, and R. R. Ruetsch, "Methods for predicting the thermal conductivity of composite systems: A review," *Polym. Eng. Sci.* **16**(9), 615–625 (1976).
- ²⁷K. Pietrak and T. S. Winiewski, "A review of models for effective thermal conductivity of composite materials," *J. Power Technol.* **95**(1), 14–24 (2015).
- ²⁸L. Gong, Y. Wang, X. Cheng, R. Zhang, and H. Zhang, "A novel effective medium theory for modelling the thermal conductivity of porous materials," *Int. J. Heat Mass Transfer* **68**, 295–298 (2014).
- ²⁹M. F. Ashby, "The properties of foams and lattices," *Philos. Trans. R. Soc., A* **364**(1838), 15–30 (2006).
- ³⁰L. Salari-Sharif, S. W. Godfrey, M. Tootkaboni, and L. Valdevit, "The effect of manufacturing defects on compressive strength of ultralight hollow microlattices: A data-driven study," *Addit. Manuf.* **19**, 51–61 (2018).
- ³¹C. Y. Zhao, S. A. Tassou, and T. J. Lu, "Analytical considerations of thermal radiation in cellular metal foams with open cells," *Int. J. Heat Mass Transfer* **51**(3-4), 929–940 (2008).
- ³²F. Clouet, "The Rosseland approximation for radiative transfer problems in heterogeneous media," *J. Quant. Spectrosc. Radiat. Transfer* **58**(1), 33–43 (1997).
- ³³Y. S. Touloukian, R. W. Powell, C. Y. Ho, and P. G. Klemens, *Thermophysical Properties of High Temperature Solid Materials* (Purdue University, 1970).
- ³⁴T. M. Tillotson and L. W. Hrubesh, "Transparent ultralow-density silica aerogels prepared by a two-step sol-gel process," *J. Non-Cryst. Solids* **145**, 44–50 (1992).
- ³⁵L. J. Gibson, Ph.D. dissertation (Churchill College, University of Cambridge, 1981).
- ³⁶M. A. Worsley, S. O. Kucheyev, J. H. Satcher *et al.*, "Mechanically robust and electrically conductive carbon nanotube foams," *Appl. Phys. Lett.* **94**, 073115 (2015).